

## FULL PAPER

# Effect of melt miscibility, polymorphism, and crystal morphology on tensile deformation of blends of isotactic polypropylene and propylene-1-hexene random copolymers

Hamed Janani<sup>1</sup>  | Rufina G. Alamo<sup>2</sup> 

<sup>1</sup>Chemical Engineering Department, Ferdowsi University of Mashhad, Mashhad, Iran

<sup>2</sup>Department of Chemical and Biomedical Engineering, FAMU-FSU College of Engineering, Tallahassee, Florida

## Correspondence

Rufina G. Alamo, FAMU-FSU College of Engineering, Department of Chemical and Biomedical Engineering, 2525 Pottsdamer St, Tallahassee, FL, USA.  
Email: alamo@eng.fsu.edu

## Funding information

National Science Foundation, Grant/Award Number: DMR1105129

## Abstract

The ductile behavior of isotactic polypropylene (iPP) can be effectively increased by blending with small contents (<25%) of a random propylene 1-hexene copolymer (PH). In this work, we have studied the uniaxial tensile deformation of binary blends of iPP with PH copolymers with 11 or 21 mol% 1-hexene. Blends iPP/PH11 are melt-miscible in the whole range of composition while iPP/PH21 blends are melt-immiscible, but partially compatible. On cooling, the lamellar morphology of each type of blend differs accordingly, and impacts their mechanical deformation. Miscible iPP/PH11 blends develop inter-mixed monoclinic lamellar stacks interconnected by tie molecules of iPP and PH admixed in the amorphous phase. During deformation, the monoclinic crystals transform to oriented mesophase at low strains due to effective stress transfer through the interconnected topology. These blends display the largest strain (~800%) and low recovery. Conversely, immiscible iPP/PH21 develop a coarser morphology of monoclinic and trigonal crystallites in the iPP-rich and PH21-rich domains, respectively. Less effective stress transfer associated with the coarse iPP/PH21 morphology leads to a delayed onset of orientation and a less effective monoclinic-mesophase transformation. The PH21 trigonal crystals of the blend orient but do not undergo polymorphic transformation. At high elongations fibrillar strain-induced trigonal crystals, provide a network of stable physical junction points that relax to the random orientation upon removal of the load, thus enhancing the elastic recovery of iPP/PH21 blends.

## KEYWORDS

iPP copolymers, iPP crystallization, iPP mechanical properties, iPP polymorphism

## 1 | INTRODUCTION

The polymorphic behavior, semicrystalline structure, and mechanical properties of isotactic poly(propylene) (iPP) change when defects or a comonomer are incorporated to the chain. The addition of a suitable content of comonomer to the iPP chain enables polypropylene materials with a wide spectrum of properties ranging from rigid thermoplastics to elasto-plastomers or to elastomers.<sup>[1]</sup>

Mixtures of iPP and propylene-1-alkene thermoplastic elastomers, form both miscible, and immiscible (but compatible) blends.<sup>[2-4]</sup> In binary blends of random atactic propylene-butene (PB) copolymers analyzed by SANS, the melt-miscibility increased with increasing difference in content of 1-butene.<sup>[5]</sup> This effect was attributed to a negative enthalpy interaction between propylene and 1-butene monomer units and to attractive entropic contributions. Based on such results, it was hypothesized that the branches longer than ethyl,

such as the butyl branch of propylene 1-hexene copolymers (PH) or the hexyl of propylene 1-octene (PO), would contribute to a more effective interaction with the iPP chain.<sup>[5]</sup> Furthermore, in our recent work on melt miscibility of iPP and PH copolymers we estimated a critical value of difference in 1-hexene content for miscibility of propylene 1-hexene copolymers of about 11 mol%. This value is close to the critical value found for miscibility of iPP/PE blends.<sup>[2–4]</sup>

The melt miscibility of iPP blends has a direct effect on their solid semicrystalline structure and mechanical behavior. The mechanical properties of miscible blends of iPP with low (0.49 mol%) and high (11 mol%) contents of stereo defects were studied by Auriemma et al.<sup>[6,7]</sup> The blends form mixed lamellar stacks with high inclusion of both components in the stacks, which is a feature supporting their miscibility at the molecular level.<sup>[6]</sup> Blends with >50 wt% of highly stereo-regular iPP are stiff materials with elastic modulus in the range of 200 to 300 MPa and yield stress ~25 to 30 MPa. It was shown that the addition of only 10 wt% stereo-irregular iPP (11 mol% defects), doubles the elongation at break to a value of ~600%, while the yield strength remained close to that of neat stereoregular iPP.<sup>[6]</sup>

It is also known that iPP, iPP copolymers, and their blends undergo polymorphic transformations under tensile deformation including  $\alpha$  (monoclinic) to mesophase,<sup>[8,9]</sup>  $\gamma$  (orthorhombic) to  $\alpha$  and  $\gamma$  to mesophase,<sup>[10]</sup> as well as  $\beta$  to  $\alpha$ .<sup>[11,12]</sup> In a recent work, we studied binary blends of propylene-1-hexene copolymers with 11 and 21 mol% 1-hexene (PH11/PH21 blends) in which the components form different crystallographic phases (monoclinic in PH11 and trigonal in PH21). We investigated the polymorphic transformation behavior under deformation of these blends.<sup>[13]</sup> The observed crystal transformations included reversible lamellar to fibrillar transformation of trigonal for PH21, or an irreversible  $\alpha$  crystal to mesophase for pure PH11 and the blends.<sup>[13]</sup> Furthermore, PH11-rich blends develop additional trigonal crystals under deformation. Such feature was explained in terms of reduced entropic barrier for the formation of trigonal crystals due to chain orientation and local enhancement of the density of short isotactic sequences.<sup>[13]</sup>

The ability of incorporating the branches in the trigonal crystalline regions of propylene 1-hexene copolymers (with >13 mol% 1-hexene) opens the window to study the effect of the trigonal phase on blends of iPP and copolymers of iPP with 1-hexene.<sup>[14–23]</sup> In an earlier study, we found that blends of iPP and PH11 are miscible in the melt in the whole range of compositions.<sup>[4]</sup> Conversely, blends of iPP and PH21 are immiscible but partially compatible. Upon crystallization, both types of blends develop two populations of crystallites. However, there should be more chain connectivity in the intercrystalline regions of the semicrystalline structure that develops from the miscible blends. Hence, an enhanced mechanical behavior is expected for the miscible blends. Moreover, the content of trigonal phase is higher in the immiscible blends, and this feature may compensate the otherwise decrease of tensile properties of the iPP/PH21 blends. The rationale is that unlike monoclinic ( $\alpha$ ) crystals that transform to mesomorphic structures under tensile deformation, PH trigonal crystals are more stable, they orient, but do not transform to the mesophase under elongation. Hence, the presence of trigonal admixed with  $\alpha$  crystals in

iPP/PH21 blends, even at low contents of PH21, may reinforce their tensile mechanical behavior.

In the present work, we address the effect of the initial state of the melt on the semicrystalline structure, and its evolution during tensile deformation, of melt miscible and immiscible iPP/PH blends. To the best of our knowledge, this is the first of such studies in iPP/PH copolymers. Understanding the mechanical behavior of the blends in reference to their semicrystalline structure will set the stage to predict the mechanical performance of other iPP blends based on the content and type of copolymer admixed with iPP.

## 2 | EXPERIMENTAL SECTION

### 2.1 | Materials

The isotactic polypropylene (iPP) and propylene 1-hexene random copolymers (PH11 and PH21) were synthesized using the metallocene catalyst described in prior works.<sup>[24–27]</sup> All polymers have very similar weight average molecular weight, in the range of 160±5 kg/mol and polydispersity index of ~2.03. Copolymers PH11 and PH21 have 11 and 21 mol% 1-hexene randomly incorporated, respectively. Binary blends of iPP with 25, 50, and 75 wt% of PH11 or PH21 were prepared in solution following the procedures described in prior works.<sup>[13,24]</sup> Films, ~250  $\mu\text{m}$  thick, of each sample were prepared by melt compression molding at 200°C for 3 minutes and cooled slowly to room temperature (23±1°C). The films were kept at room temperature for at least 2 weeks prior to any testing.

### 2.2 | Uniaxial tensile deformation test

The samples were cut into dumbbell shapes with necking width, gauge length, and thickness dimensions of 2 mm×5.5 mm × 0.25 mm, respectively. A Thümler tensile test machine model TH 2730 was used for the stress-strain measurements at the drawing rate of 25 mm/min. The distance,  $l$ , between two bench marks drawn on the necking region of samples was measured and the engineering strain,  $\epsilon$ , was obtained based on the initial distance between the bench marks,  $l_0$ , as  $\epsilon = \frac{l-l_0}{l_0} \times 100$ . The engineering stress was calculated as the force per initial cross sectional area. The elastic modulus ( $E$ ), yield stress ( $\sigma_y$ ), tensile strength ( $\sigma_b$ ), and elongation at break ( $\epsilon_b$ ) were all obtained from the stress-strain curves as described elsewhere.<sup>[13]</sup> The recovered strain after break,  $r_b$ , was also recorded as a measure of the elastomeric behavior of the blends.  $r_b$  was calculated as  $r_b = \frac{L_f - L_b}{L_b} \times 100$  where  $L_f$  is the final length at break and  $L_b$  is the total length of broken pieces after break. The reported values are averages for over five independent experiments.

### 2.3 | Polymorphic transitions under deformation

A house-made stretching device was built and installed inside the sample compartment of the Bruker Nanostar diffractometer to

study the change of crystal structure under deformation. The dumbbell-shaped sample was stretched to a specific strain and WAXS/SAXS patterns were collected simultaneously while under tension. In order to reduce the effect of air scattering, vacuum of ~3 mbar was applied to the sample compartment. After collecting the patterns, the vacuum was released and the WAXS detector (Fuji Film image plate) was scanned using a Fuji FLA-7000 scanner to obtain the 2D WAXS pattern. The sample was stretched then to a higher strain and this procedure continued up to the breaking strain of the sample.

## 2.4 | Melting

The melting thermograms of nonstretched samples cooled to room temperature from melt and aged for 2 weeks, were recorded using a TA instrument DSC Q2000 connected to an intercooler. The instrument operates under dry nitrogen and was calibrated for temperature and heat flow with indium. The applied thermal history was a standard melting-cooling-melting cycle in the temperature range of  $-50$  to  $200^{\circ}\text{C}$  at a constant rate of  $10^{\circ}\text{C}/\text{min}$ .

## 3 | RESULTS AND DISCUSSION

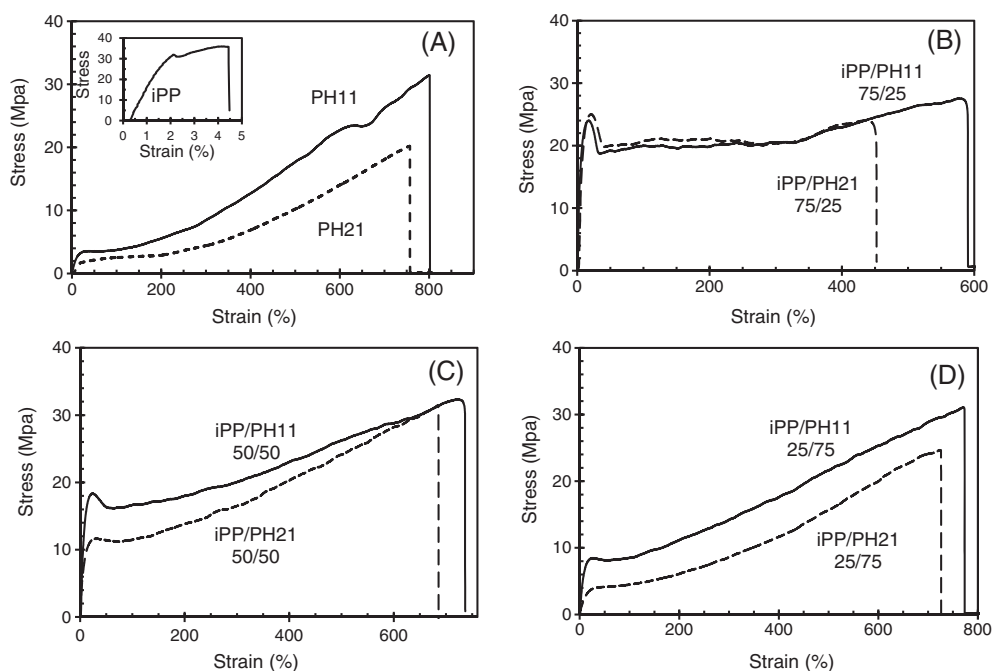
This section is divided as follows, in section 3.1 the major features of the tensile stress-strain behavior of all iPP/PH11 and iPP/PH21 blends are first discussed comparatively. We continue in section 3.2 with a more detailed polymorphic and structural analysis during tensile deformation from the recorded WAXS, SAXS, and DSC patterns. Finally, on the basis of the observed structural and polymorphic

changes, we explain in section 3.3 the differences found in tensile behavior.

### 3.1 | Tensile behavior of iPP/PH blends

The tensile stress-strain behavior of iPP/PH11 and iPP/PH21 is shown comparatively at identical blend compositions in Figure 1. The behavior of the pure components is given in Figure 1A. Neat iPP undergoes very small tensile deformation ( $<5\%$ ) before failure. PH11 and PH21 are thermoplastic elastomers with relatively low modulus but high elongation at break (750–800%). A major feature of the mechanical behavior upon blending is that even small contents of the copolymer confer elastomeric properties to the iPP blend, as seen in Figure 1B. Here, the iPP/PH 75/25 blends deform up to high strains ( $>450\%$ ) while maintaining the characteristic high elastic modulus of iPP. Increasing the content of PH copolymer in the blend has a negative effect in the moduli that decreases proportionally to the PH content but the elongation increases as seen in panels (C) and (D) of Figure 1. The stress at break is basically invariable for all blends ( $\sim 32$  MPa for iPP/PH11 and  $\sim 25$  MPa for iPP/PH21). At relatively high strains, the deformation of blends and copolymers follows a clear strain-hardening behavior, that appears enhanced in the copolymer-rich blends. Furthermore, at the same composition, the elongation at break is systematically higher in PH11-containing blends compared to iPP/PH21. The difference in elongation is more significant at the lower contents of PH copolymer, such as in blends with 25 wt% PH (Figure 1B).

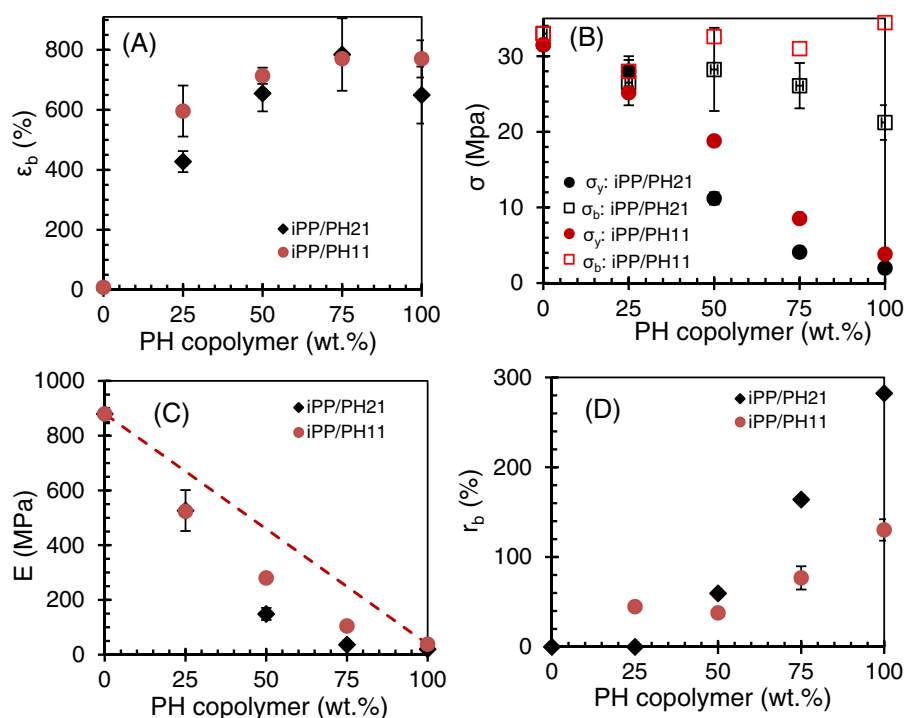
Detailed mechanical property data, extracted from the stress-strain curves, including elastic modulus  $E$ , yield stress  $\sigma_y$ , tensile stress at break  $\sigma_b$ , elongation at break,  $\epsilon_b$ , and the elastic recovery at break,



**FIGURE 1** Stress-strain graphs of neat polymers, A, and iPP/PH blends B–D. Continuous lines describe iPP/PH11 blends and dashed lines correspond to iPP/PH21 blends

**TABLE 1** Mechanical properties obtained from stress-strain behavior of the blends

Type	Comp.	Elastic modulus (MPa)	Yield stress (MPa)	Stress at break (MPa)	Strain at break (%)	Strain recovery after break (%)
iPP/PH11	0/100	38 ± 9.2	3.9 ± 0.5	34 ± 6	770 ± 62	130 ± 12
	25/75	105 ± 12	8.6 ± 0.1	31	770 ± 1	77 ± 13
	50/50	280 ± 5	18.8 ± 0.8	32.6 ± 0.8	714 ± 27	38
	75/25	524 ± 15	24 ± 1	31.8	596 ± 85	45
	100/0	880 ± 20	-	33	8	-
iPP/PH21	0/100	21 ± 1	2 ± 0.3	21 ± 2.3	650 ± 95	282
	25/75	37.1 ± 2	4.1 ± 0.1	26 ± 3	785 ± 121	164
	50/50	149 ± 22	11.2 ± 0.8	28 ± 5	655 ± 60	38
	75/25	527 ± 5	28 ± 2	27 ± 3	427 ± 35	-
	100/0	880 ± 20	-	33	8	-

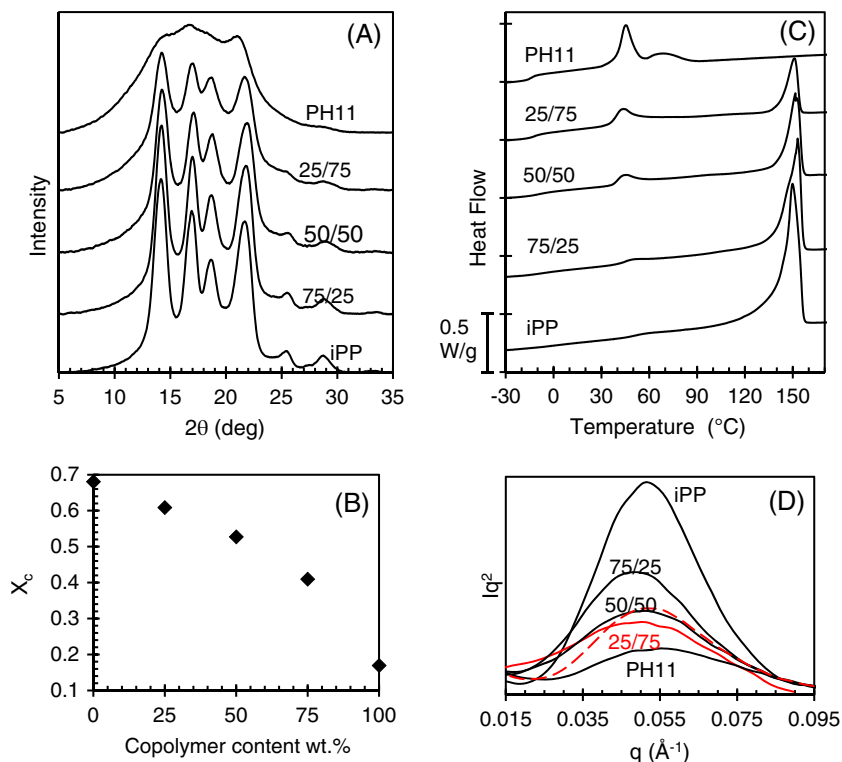
**FIGURE 2** Mechanical properties extracted from stress-strain plots of iPP/PH11 and iPP/PH21 blends against blend composition. A, elongation at break  $\epsilon_b$ , B yield stress,  $\sigma_y$ , and tensile strength,  $\sigma_b$ , C, elastic modulus  $E$ , and D, elastic recovery after break,  $r_b$ 

$r_b$ , are compared for the two types of blends in Table 1 and shown graphically in Figure 2 as a function of increasing comonomer content.

The yield stress decreases from  $33 \pm 2$  MPa (for neat iPP) to  $24 \pm 1$  MPa for iPP/PH21 25/75 wt% and to  $28 \pm 2$  MPa for iPP/PH11 25/75 wt% with increasing PH content (Figure 2B). The yield strength is generally higher in iPP/PH11 compared to iPP/PH21 blends (Figure 2B). It is clear in Figure 1A that yield stress of PH11 is higher compared to PH21, although the overall degree of crystallinity is slightly lower (see Section 3.2). Higher yield strength is consequently observed in the blends of iPP/PH11 compared to iPP/PH21 at same blend composition. The elastic modulus decreases from  $880 \pm 20$  MPa (for neat iPP) to  $21 \pm 1$  MPa (iPP/PH21 25/75 wt%) and to  $38 \pm 9$  (iPP/PH11 25/75 wt%) with increasing PH copolymer in the blends (Figure 2C). The elastic modulus of the blends is lower than the

calculated weighted average of the Young's moduli of the neat components (dashed line in Figure 2C). The elastic modulus of blends of two semicrystalline polymers depends on type and content of crystal phase from each constituent and the degree of connectivity between the crystallites.<sup>[6]</sup> Despite the lower elastic moduli and yield strength of the blends compared to neat iPP, they show similar ultimate tensile strength (~30 MPa) due to the significant strain hardening with increasing copolymer content in the blends. The difference between stress at break and stress at yield ( $\sigma_b - \sigma_y$ ) increases with PH content for both types of blends due to the significant strain hardening (Figure 2B). The ultimate stress is very close to the yield stress in the 25% blends, but is slightly higher in iPP/PH11 since it shows some strain hardening at this composition. The difference in ductile behavior between iPP/PH11 and iPP/PH21 can be better understood on

**FIGURE 3** iPP/PH11 blends crystallized at room temperature: A, WAXD diffractograms, B, crystallinity level vs blend composition, C, melting thermograms, and D, Lorentz-corrected SAXS patterns. Dashed red line in panel D represents the calculated SAXS profile for iPP/PH11 25/75 by adding the patterns of neat iPP and PH11 proportionally to their weight fraction



the basis of changes in crystal structure under deformation as will be discussed later in Section 3.2.

The elastic recovery,  $r_b$ , was estimated in order to compare the elasticity of the two types of blends quantitatively. Elastic recovery is plotted vs PH content in Figure 2D. PH21 shows significantly higher elasticity with  $r_b \sim 300\%$  and PH11 shows an elastic recovery of  $\sim 130\%$ . In the same manner, PH21 containing blends show higher elasticity behavior compared to iPP/PH11 blends, especially for the 75 wt% PH blends. In other words, stretched chains of PH21 at high elongations have more tendency to relax to random conformation upon removing the load.

In summary, the tensile stress-strain study showed that thermo-plastic elastomers PH11 and PH21 could effectively enhance the ductile behavior of iPP upon blending with these components. Compared to the immiscible iPP/PH21 blends, the miscible iPP/PH11 blends show higher elongation at break especially at low PH11 content with strain values of 600% to 800% vs 400% to 600% for iPP/PH21 blends. Conversely, iPP/PH21 blends show significantly higher elasticity particularly in PH-rich blends.

### 3.2 | Crystal transformation under deformation in iPP/PH blends

In order to properly map the semicrystalline structure with the tensile behavior of the blends, the initial type and content of polymorphic phases in the nondeformed state as well as the transformation of such structures during deformation need to be characterized. The initial

state of the melt and the possibility of iPP and PH copolymers to cocrystallize or to form separated phases affects the connectivity of lamellae stacks, which will impact the mechanical performance of the blends.

We first start with melt homogeneous blends in which both components crystallize in the same monoclinic phase; these are the iPP/PH11 blends. WAXS patterns of the initial blends for all blend compositions are shown in Figure 3A. iPP and PH11 both form monoclinic crystals as indicated by the characteristic reflections of  $(110)_\alpha$ ,  $(040)_\alpha$ , and  $(130)_\alpha$  planes appearing at  $2\theta$  of  $14^\circ$ ,  $16.8^\circ$ ,  $18.8^\circ$ , respectively, as well as planes  $(111)_\alpha$  and  $(041)_\alpha/(131)_\alpha$  clustered in a relatively broad peak at  $21^\circ$  to  $22^\circ$ .<sup>[25]</sup> As shown, the blends display identical characteristic reflections. The degree of crystallinity estimated by subtracting the halo of an amorphous polypropylene at room temperature, was  $\sim 70\%$  for iPP,  $\sim 17\%$  for PH11 and intermediate values for the blends as shown in Figure 3B. Despite the melt miscibility and the fact that both iPP and PH11 form monoclinic crystals, due to large differences in crystallization kinetics,<sup>[14]</sup> the DSC melting thermograms (Figure 3C) show double melting peaks for the blends, evidencing the formation of at least two populations of crystallites, iPP-rich and PH11-rich lamellae stacks.

Figure 3D shows the Lorentz corrected SAXS data of iPP/PH11 blends. Applying the one-dimensional correlation function to these data, the average lamellae thickness ( $l_c$ ) was estimated as 72 and 52  $\text{\AA}$  for iPP and PH11, respectively. The obtained  $l_c$  values are in close agreement with values of 88 and 50  $\text{\AA}$  previously reported in literature for similar metallocene iPP and PH11.2 crystallized under similar conditions.<sup>[9]</sup> In the SAXS patterns, the position of the correlation

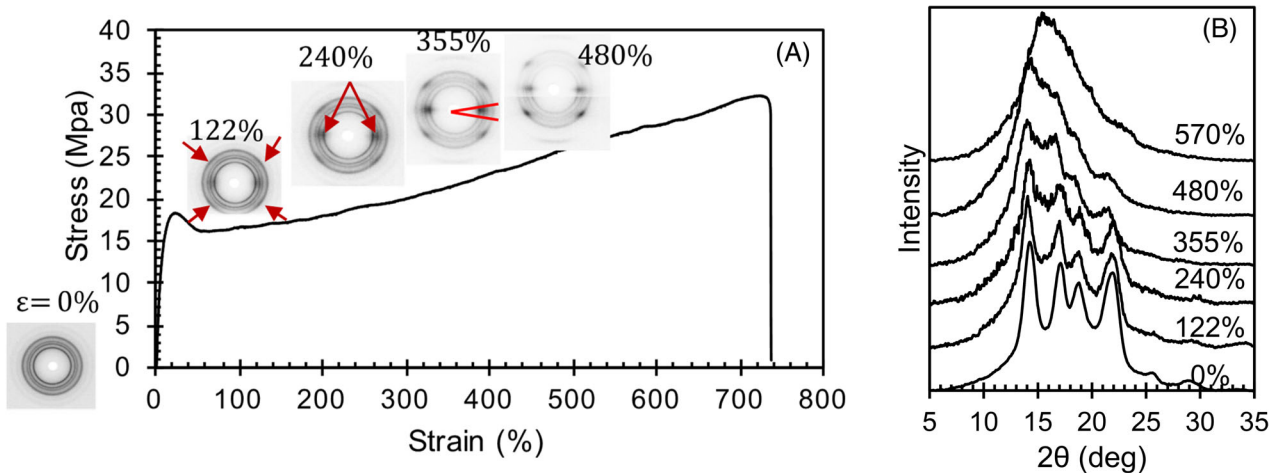


**FIGURE 4** A, Structure evolution under tensile deformation for iPP/PH11 50/50 wt% with corresponding 2D WAXS patterns. B, 1D WAXS patterns integrated in the azimuthal equatorial region highlighted in the 2D WAXD pattern at  $\epsilon = 355\%$ . The red arrows indicate the onset of stress-induced mesophase formation (122% strain)

peak and its shape are dominated by the major component in the blend. In addition, with increasing content of PH11, the width of the correlation peak broadened, and the intensity is lowered, especially in the composition range of 25 to 50 wt% of PH11. If each component of the blend forms a cluster of separated lamellae stacks, then the position of the maxima associated with each component in the blend would appear at the same position as for the neat polymers, and the scattered intensity from different clusters would contribute additively to the total intensity.<sup>[7]</sup>

Although difficult to model, a test for mixed lamellae is shown by the red dashed line in Figure 3D for iPP/PH 25/75. It was calculated by adding the SAXS profiles of the pure components proportionally to their weight fraction in the blend. The calculated profile is narrower and shifted to slightly higher  $q$  compared to the actual pattern of the blend. The difference supports the formation of mixed lamellae stacks with increased connectivity. Broadening of the correlation peak in the experimentally obtained pattern can be explained by the higher state of disorder within the lamellae stacks of the blend as it was also observed in miscible blends of iPP with different levels of stereoregularity reported by Auriemma et al.<sup>[7]</sup> When the degree of inclusion of both components in the lamellae stacks becomes identical, a weak correlation peak (or no peak at all) may be observed.<sup>[7]</sup> Auriemma's results resemble the SAXS behavior of miscible iPP/PH11 blends of this work. Hence, the formation of an interconnected lamellar structure with random inclusion of lamellae of both components within a stack, is inferred from the observed experimental SAXS data. The slight decrease of long period with increasing content of PH11 also supports the formation of intercalated lamellae of iPP and PH11 in the crystal stacks.

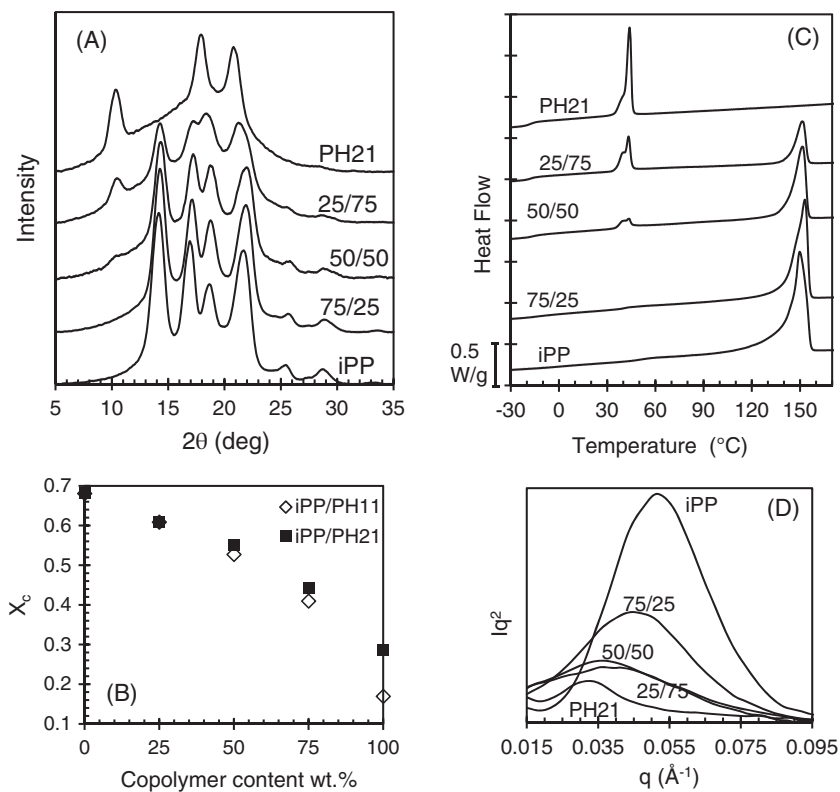
The change in crystal structure of iPP/PH11 blends under tensile deformation is analyzed next. A representative behavior is shown in Figure 4A for the 50/50 wt% blend where 2D WAXD patterns are given at different stages of the tensile deformation. The behavior of the rest of the blends can be found in Figure S1. The 1D WAXD patterns integrated along the equatorial line (perpendicular to the

stretching direction), in the azimuthal region between  $75^\circ$  and  $105^\circ$ , are given in Figure 4B. The azimuthal range used for integration is illustrated on the 2D WAXS of the blend at  $\epsilon = 355\%$ . The general characteristics of the crystal transformations during deformation are similar for all blend compositions. The beginning of orientation is coupled with transformation of the monoclinic to mesophase. Orientation develops shortly after yield as indicated by the appearance of  $(111)_\alpha$ ,  $(041)_\alpha/(131)_\alpha$  reflections in the azimuthal angle  $\sim 42^\circ$ , forming the six point reflection pattern characteristic of stress-induced mesophase.<sup>[28]</sup> A characteristic of this transformation is broadening of  $(110)_\alpha$ ,  $(040)_\alpha$  and  $(130)_\alpha$  reflections along the equator until they merge into a single halo in the  $2\theta$  range of  $14$  to  $16^\circ$  (indicated by a red arrow in Figure 4A).

The complete transformation from monoclinic crystals to mesophase found for neat iPP,<sup>[29]</sup> does not occur in these iPP blends. Even at very high elongations, weak isotropic rings corresponding to the reflections of randomly oriented monoclinic lamellae remain. One should also note the development of a broad reflection at  $2\theta = 10.5^\circ$  in the 2D patterns of blend iPP/PH11 25/75 at elongations  $>150\%$  (Figure S1). This reflection is the signature of the trigonal phase found in un-oriented PH copolymers with  $>15$  mol%.<sup>[9]</sup> Trigonal crystals were also found to develop in pure PH11 under deformation as a consequence of a decrease in the entropy barrier for formation of this phase at high elongations.<sup>[13]</sup>

WAXS diffractograms of the initial iPP/PH21 blends are given in Figure 5A. PH21 crystallizes in the trigonal phase ( $\delta$  phase) as seen by the three major reflections of planes  $(110)_\delta$ ,  $(300)_\delta$ ,  $(220)_\delta$ , and  $(211)_\delta$  at  $2\theta = 10.5^\circ$ ,  $17.5^\circ$ ,  $20.3^\circ$ , and  $20.6^\circ$ .<sup>[16,17]</sup> For blends with  $>25$  wt% PH21, the characteristic reflections of the trigonal and monoclinic phase  $(130)_\alpha$  at  $2\theta \sim 18.8^\circ$  are observed. Blends with  $\leq 25$  wt% PH21 show similar phase structure as neat monoclinic iPP with no detectible trigonal. The level of crystallinity extracted from the WAXD patterns for the two sets of blends is shown comparatively as a function of blend composition in Figure 5B. Due to the formation of the trigonal

**FIGURE 5** iPP/PH21 blends crystallized at room temperature. A, WAXD diffractograms, B, crystallinity level of both blend types vs blend composition, C, melting thermograms, and D, Lorentz-corrected SAXS patterns



phase, the level of crystallinity of PH21 (28%) is higher than the crystallinity level of PH11 (17%) in spite of the higher comonomer content. This difference is also reflected in the overall crystallinity levels of comonomer rich blends, as seen in this figure.

Similar to iPP/PH11 blends, the DSC melting of iPP/PH21 (Figure 5C) shows double melting peaks associated with at least two populations of crystallites, in this case the trigonal form of PH21 and the monoclinic of iPP. In a previous work, we showed that in the immiscible blends of iPP/PH21, the nonisothermal crystallization temperature decreases slightly with increase in PH21 content of the blend. In Figure 5C, it is also noticed that in the blends, the iPP-rich domain melts at decreasing temperatures with increasing PH21 in the blend. The latter is expected if the PH21 content increases in this domain. The observed trends are indicative of some level of compatibility between iPP and PH21 in the iPP-rich and PH21-rich liquid-liquid phase separated domains, especially at high contents of PH21.

The SAXS patterns (Figure 5D) show a large difference in long period between lamellae stacks of trigonal in PH21 and the monoclinic lamellae of iPP (19 and 11 nm, respectively). In the blends, the average long spacing increases with increasing content of PH21, as indicated by the shift of the SAXS peak to lower  $q$  values. A reversed trend was observed previously in the case of miscible iPP/PH11 blends. Due to phase separation in the melt, it is expected that crystallization occurs separately in iPP-rich and PH21-rich domains. Consequently, there is less or no probability of intercalated lamellae structures of iPP and PH21. The formation of isolated trigonal and monoclinic stacks in the blends add up to the observed increase in long spacing with increasing PH21 content.

The evolution of crystallographic structure under tensile deformation of the iPP/PH21 blends is shown in Figure 6 where data for the 50/50 blend is given as a representative example. Similar plots can be found in Figure S2 for the rest of the iPP/PH21 blends. A monoclinic to mesophase transformation with similar diffraction characteristics as described for iPP/PH11 blends is also observed for iPP/PH21 blends but in the latter the onset is at higher strains ( $>100\%$ ). The isolated trigonal reflection at  $2\theta = 10.5^{\circ}$  is ideal to monitor the transformation of this polymorph independently from the transformation of the monoclinic phase. As shown in the 1D patterns of Figure 6B, unlike monoclinic crystals, trigonal crystals do not undergo polymorphic transitions under deformation. Orientation of trigonal lamellae and transformation into a fibrillar structure occurs mainly in the strain hardening region as indicated by high intensity dots at  $2\theta = 10.5^{\circ}$  in the equator of the 2D WAXD patterns. Furthermore, changes in the intensity of the equatorial reflection at  $2\theta = 10.5^{\circ}$  which increasing strain is indicative of the formation of additional stress-induced trigonal crystals under deformation as described previously.<sup>[13]</sup>

The structural transformation from isotropic crystals to oriented structures with increasing strain occurs more gradually in iPP/PH21 blends compared to iPP/PH11. For example, for iPP/PH21 75/25 wt %, the WAXD pattern is isotropic even at  $\epsilon = 90\%$ , well above the yield strain (Figure S2), while for iPP/PH11 75/25 wt%, the formation of mesophase and/or aligned crystals is evident at  $\epsilon = 40\%$ , by the anisotropic pattern intensified at the equator (Figure S1). Similarly, the 2D SAXS patterns of iPP/PH11 75/25 show no correlation peaks even at low strains of  $\epsilon = 40\%$ , which indicates that the long periodicity between lamellar stacks becomes diffuse in the presence of

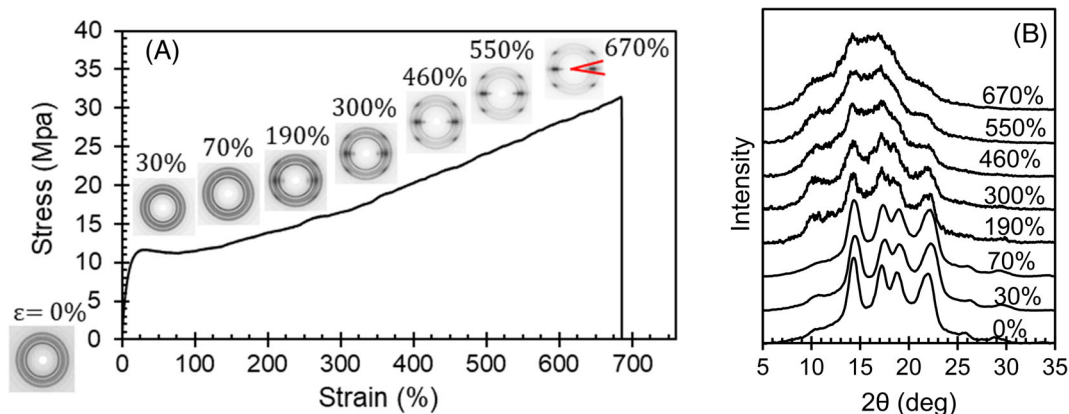


**FIGURE 6** A, Structure evolution under tensile deformation for iPP/PH21 50/50 wt% with corresponding 2D WAXS patterns. B, 1D WAXS patterns integrated in the azimuthal direction of the equatorial region (highlighted area on 2D WAXD at  $\epsilon = 670\%$ )

mesophase. However, iPP/PH21 75/25 shows a clear correlation peak (red halo) at  $\epsilon = 90\%$  (see Figure S3). Hence, the hierarchical lamellar structure is effectively distorted in iPP/PH11 blends compared to iPP/PH21, even at low strains close to the yield point.

### 3.3 | Discussion of tensile deformation in iPP/PH blends

The structural mechanism of plastic deformation in semicrystalline polymers has been described from different views.<sup>[30–33]</sup> In a model suggested by Men and coworkers, a semicrystalline polymer is considered as a composite of two interpenetrating networks between interconnected lamellae blocks and the entangled amorphous network.<sup>[34]</sup> The critical aspects of the true stress-strain curves of such polymers include,<sup>[34–38]</sup> local intralamellar slip processes just before yield and after a purely elastic deformation (point A), and a change into a collective activity of slip motions all over the lamellae at the yield point of the polymer (point B). On further strain, lamellae disaggregation and chain unfolding (also referred to as mechanical melting) and recrystallization into fibrillar structures occur (point C).<sup>[34]</sup> The disentanglement and cavity formation occurs at very high deformations close to the breaking point (point D). The strain at points A and B are related to the properties of the crystal phase, independently from the entangled state of the amorphous network, however, the strain at point C is determined by the interplay between the stability of crystals and entanglement density in the amorphous phase. It has been reported for the immiscible blends of iPP with olefin block copolymers (OBC) elastomers that compared to neat iPP, the cavitation mechanism was promoted at very high elongations.<sup>[39]</sup> Cavitation is enhanced by a less-uniform stress distribution, particularly by stress concentration at the interface of phase separated polymers.<sup>[39]</sup>

Based on the unified vision presented above for deformation of semicrystalline polymers, the discussion of the structure-deformation behavior of iPP/PH blends is organized to cover tensile properties at strains around the yield point, followed by the strain-softening region ( $0 < \epsilon < 100\%$ ), and finally the properties at higher strain regimes ( $\epsilon > 100\%$ ) including strain hardening up to the breaking point.

#### 3.3.1 | Deformation at $0 < \epsilon < 100\%$

Despite a similar level of crystallinity of iPP/PH11 and iPP/PH21 blends (Figure 5B), the elastic moduli and yield stresses are generally higher in iPP/PH11 compared to iPP/PH21 blends (Figure 2B, C). Hence, the difference must be related to the types of crystalline structures formed in each type of blend. We have shown that PH11 displays higher yield stress and modulus than PH21, despite a slightly lower crystallinity and thinner lamellae (6 and 11 nm for PH11 and PH21, respectively).<sup>[13]</sup> We explained this apparent anomaly as the ability of the defect-free monoclinic crystals of PH11 to resist better the applied force compared to the trigonal crystals of PH21 which have lower packing density due to inclusion of the side branches in the crystal.<sup>[13]</sup> Consequently, local slips within the crystals that are considered the beginning of yielding are energetically favored for iPP/PH21 blends compared to iPP/PH11.

The other major observation in this region was the significant orientation observed in 2D WAXS of iPP/PH11 blends at strains as low as 40% while isotropic WAXS patterns indicative of a randomly oriented lamellar structure are found in iPP/PH21 even at  $\epsilon \approx 100\%$  (Figures 4 and 6). A different initial lamellar structure explains the difference in onset of orientation. Partially cocrystallized and intercalated lamellar stacks of iPP-rich and PH11-rich molecules which are interconnected with an amorphous phase of iPP and PH11 chains admixed at the molecular level, effectively provides a network of physical crosslinks that transfers efficiently the stress to the crystallites. Hence, the change of local slips into collective slips of crystal blocks and their orientation are relatively fast in iPP/PH11 blends. On the other hand, clustered lamellae stacks formed from the liquid-liquid phase separated domains in the nonstretched iPP/PH21 are not connected by a homogeneous amorphous phase. Therefore, although the activation energy for local slips within the PH21 crystalline cluster may be lower than in the iPP/PH11 blends, the overall change into collective slips is hindered by lack of chain connectivity at the interface. Hence, the overall lamellar structure is preserved in the iPP/PH21 blends even above the yield point ( $\epsilon \approx 90\%$ ) as supported by

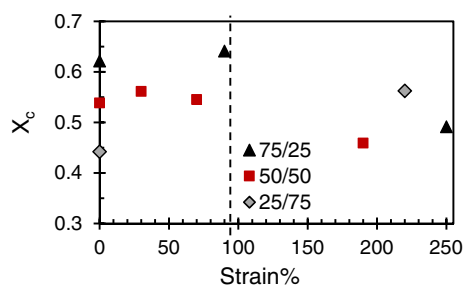


**FIGURE 7** Overall crystallinity level against strain during uniaxial tensile deformation of iPP/PH21 blends

the presence of the SAXS correlation peak (Figure S3). In addition, the estimated degree of crystallinity before and after yield ( $0 < \epsilon < 100\%$ ) for iPP/PH21 blends (50/50 and 75/25) shows no significant change (Figure 7).

### 3.3.2 | Deformation at $\epsilon > 100\%$

Three major differences observed for the two types of blends at high elongations include: higher elongation at break in iPP/PH11 blends, slightly higher strain hardening behavior in iPP/PH21 blends, and finally a significantly higher recovery after break in iPP/PH21 blends compared to their iPP/PH11 counterparts. Based on the model proposed by Men and other researchers, this range of elongations corresponds to disaggregation of crystal blocks<sup>[8,34,40,41]</sup> or chain-unfolding<sup>[42]</sup> (also called mechanical melting), and recrystallization into fibrillar crystals under tensile deformation. Since the primary randomly oriented hierarchical structures are almost distorted in this range of strains for both types of blends (Figure S1 and S2), the major differences in tensile behavior of the blends at  $\epsilon > 100\%$  are driven either by the melt phase separated morphology or by type and level of crystallographic transformations under large deformations.

The formation of phase separated domains in immiscible polymer blends is always associated with the issue of interfacial adhesion between the two phases, particularly when stretched under tensile deformation, due to the possibility of cavity formation at the interface. The lower elongation at break in phase separated iPP/PH21 blends could be attributed to some cavitation at the interface of harder-softener domains at elongations close to the breaking point.<sup>[38]</sup> Indeed, it is known that enhancing the compatibility of elastomeric domains with the iPP matrix improves elongation at break.<sup>[43]</sup> For iPP/PH11 blends, however, the cavitation is less of an issue due to a more homogeneously entangled amorphous phase.

The strain hardening at high elongations in iPP/PH11 and iPP/PH21 blends, characterized by the slope of stress-strain curve in this region, is very similar for both types of blends at a fixed blend composition, but slightly higher for iPP/PH21 blends. It was shown in our previous work that the type of crystallographic transformation determines the tensile behavior for PH11/PH21 blends under high deformations.<sup>[13]</sup> PH11-rich blends show the highest strain-hardening

behavior that is enhanced by strain-induced trigonal formation and monoclinic-mesophase transformation, due to fast kinetics of chain reorganization under deformation.<sup>[13]</sup> As the content of PH21 increases, no significant polymorphic transformation was observed and the only chain re-organization event is a reversible morphological transformation of lamellar to fibrillar trigonal crystals.<sup>[13]</sup> Similarly, a slightly higher strain hardening seen in the iPP/PH21 blends may be due to the mentioned synergistic effect of monoclinic to mesophase transformation and additional development of trigonal, as explained earlier for blends of PH11 and PH21.<sup>[13]</sup>

The third difference at high elongations is in elasticity measured by the elastic recovery at break ( $r_b$ ).  $r_b$  is double for PH21-containing blends compared to iPP/PH11 blends, especially at PH contents  $> 50$  wt%. This observation may be related to the type of crystal transformation that takes place during the mechanical-melting and recrystallization to fibrillar structure. It was discussed in the previous section that both iPP/PH copolymers show the monoclinic-mesophase transformation typical of iPPs, and that iPP/PH21 shows an additional strain-induced trigonal formation. In order to gain a better understanding of different elastic behavior of the blends in the strain-hardening region, we have further quantified the level of transformation with increasing strain in both types of blends.

The content of oriented mesophase and trigonal crystals evolved during elongation was extracted from the 1D WAXD profiles. We start with iPP/PH11 blends since for these blends there is only one type of crystal transformation, that is, monoclinic to mesophase. The content of each phase at different elongations cannot be estimated from 1D WAXD patterns by regular curve fitting methods because of the overlapping reflections from monoclinic and mesophase. The level of monoclinic to mesophase transformation can be characterized by the broadening of the monoclinic reflection peaks; such broadening occurs due to distortion of the original lamellae under deformation followed by formation of disordered mesophase. Figure 8A shows the halo subtracted WAXS of iPP/PH11 50/50 at different strains, as an example. The change in height between reflections  $(110)_\alpha$  and  $(040)_\alpha$  can be used to quantify the evolution of mesophase at expenses of monoclinic crystals. As shown in Figure 8A, during the  $\alpha$ -to-mesophase transformation, the denoted difference in height decreases due to overlapping of  $(110)_\alpha$  and  $(040)_\alpha$  peaks with the broad peak of mesophase at  $2\theta = 14$  to  $16^\circ$ . The level of  $\alpha$ -to-mesophase transformation,  $X_{\text{transf}}$ , was characterized by the percentage decrease from the original height as  $X_{\text{transf}} = \frac{H_0 - H}{H_0} \times 100$ . The  $X_{\text{transf}}$  vs strain for all iPP/PH11 blends is given in Figure 8B. As shown, the transformation is higher and faster in iPP-rich blends. Very high levels of transformation ( $X_{\text{transf}} \approx 90\%$ ) of the initial monoclinic crystals to mesomorphous are observed in iPP/PH 75/25. For iPP/PH11 blends the stress is effectively transferred to all monoclinic lamellae through a homogeneously entangled amorphous phase. The stress-induced mesophase is a stable structure due to its high entropy (randomness of packing and helices), and remains as such even after removing the stress. In the absence of stress-induced trigonal physical joints in the iPP-rich blends, the elastic recovery of iPP/PH11 blends is lowered.

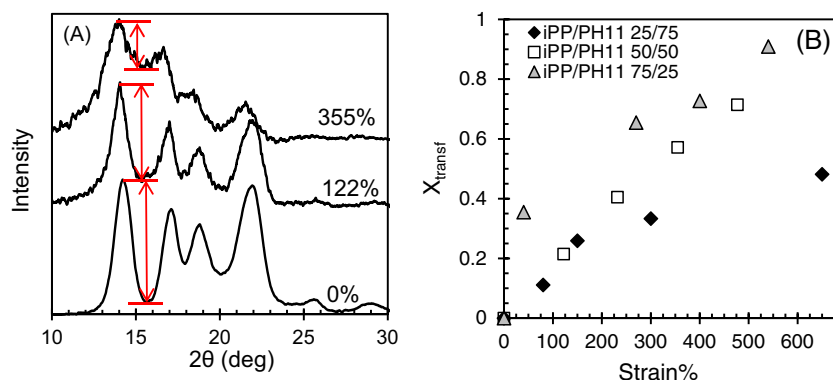


**FIGURE 8** A, Halo subtracted WAXS patterns of iPP/PH11 50/50 blend at different elongations, B, level of transformation vs strain%

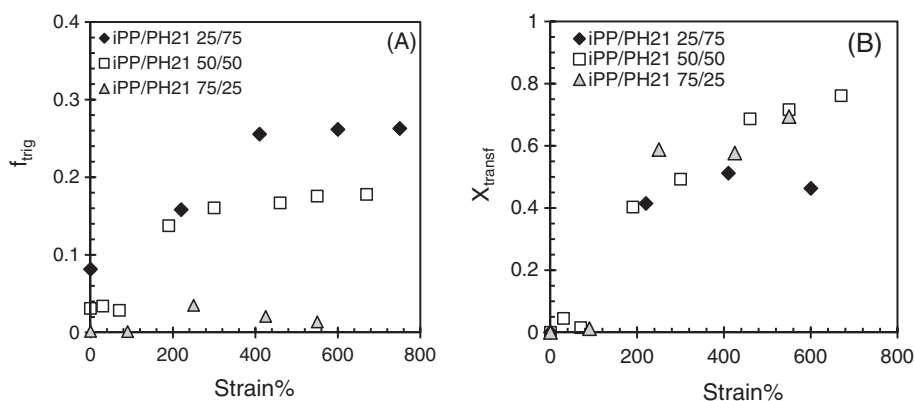


**FIGURE 9** A, Trigonal crystallinity factor and B, level of monoclinic to mesophase transformation vs strain

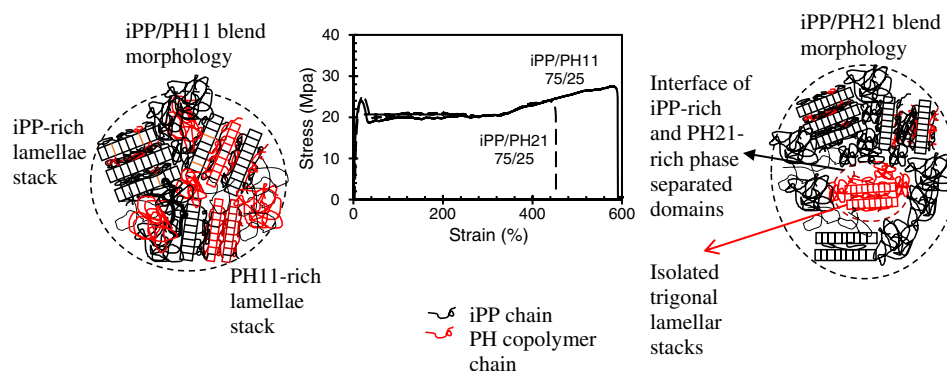
The level of monoclinic-mesophase transition,  $X_{\text{transf}}$ , for iPP/PH21 blends can also be quantified using the same method described for iPP/PH11 blends. The maximum transformation is estimated at about 70% for iPP/PH21 75/25 and 45% for 25/75 blend. The level of strain-induced trigonal formation in these blends is estimated by the trigonal crystallinity factor,  $f_{\text{trig}}$ , or the ratio of the area under peak at  $2\theta = 10.5^\circ$  to the total area in the halo-subtracted diffractogram.  $f_{\text{trig}}$  is a parameter associated with the content of trigonal crystals.<sup>[13]</sup>  $f_{\text{trig}}$  and  $X_{\text{transf}}$  at different strains are plotted in Figure 9 for iPP/PH21 blends. Both types of transformations increase significantly above  $\epsilon = 100\%$ . From the data of Figure 9, it appears that both transformations start simultaneously.  $f_{\text{trig}}$  increases as the chains become more aligned in the stretching direction due to lowering of the entropic barrier for fibrillar trigonal crystallization until it finally levels off when the supply of short isotactic sequences that form trigonal crystals is depleted. These are isotactic sequences with length in the range of 3 to 7 units, as described previously.<sup>[24]</sup> After trigonal saturation, the chains may continue orientation in the stretching direction.

The  $X_{\text{transf}}$  in iPP/PH21 is slightly lower compared to the iPP/PH11, especially at strains close to the breaking point. At a specific blend composition, it was expected that the level of transformation of  $\alpha$ -to-mesophase would be the same for both types of blends, under identical tensile deformation conditions (eg, at a specific strain and strain rate). However, as mentioned before, trigonal crystals are less resistant against external load and start to transform from lamellar

structure into oriented fibrillar structures dissipating some of the applied stress. Consequently, part of initial monoclinic lamellae in iPP/PH21 remains intact and do not transform to mesophase. Upon removal of the load, the network of fibrillar stress-induced trigonal crystals act as physical junction points (crosslinks) and tend to relax to the random orientation due to high flexibility of PH21 chains as explained previously.<sup>[13]</sup> A similar elasticity reinforcement of lamellar crystals by gamma fibrils has been reported by Men and coworkers for propylene-ethylene random copolymers (12 mol% ethylene) stretched at high temperatures ( $63^\circ\text{C}$ ) in the high deformation regime ( $\epsilon > 130\%$ ).<sup>[44]</sup> The copolymer crystallizes in a mixture of  $\alpha$  and  $\gamma$  phases. No stress-induced mesophase was observed when it was stretched at  $63^\circ\text{C}$  (above the melting temperature of mesophase), instead, stress-induced  $\gamma$  fibrils from short isotactic sequences were formed at high levels of deformation ( $130\% < \epsilon < 160\%$ ).<sup>[44]</sup> The unexpected elasticity reinforcement at high strains was explained as formation of an entangled network embedded by the stress-induced  $\gamma$  fibrils.<sup>[44]</sup>

Due to the relevance of the initial semicrystalline lamellar morphology in the uniaxial tensile deformation behavior of the iPP blends studied, we summarize the behavior with schematics of the lamellar superstructures and corresponding stress-strain deformation in Figure 10. Blends with 75% iPP are taken as representative examples. Melt miscibility of the iPP/PH11 blends in the whole concentration range, leads to a mixed monoclinic lamellar structure and a high degree of molecular mixing of both components in the interlamellar

**FIGURE 10** Schematics of the initial lamellar morphology, and stress-strain deformation, of iPP/PH11 and iPP/PH21 blends. Blends with 25% copolymer are shown as representative examples. Black lamellae are formed mainly by iPP-chains and red lamellae are formed by PH chains



regions. Hence, even if each component develop their own lamellae due to large differences in crystallization kinetics, highly oriented structures are enabled via a monoclinic to mesomorphic transformation from the early stages of deformation.

Blends of iPP/PH21 display liquid-liquid phase separation as shown in the schematics by domains of iPP-rich crystals separated from those of PH21-rich crystallites. Upon crystallization, iPP-rich domains develop monoclinic crystals, while the trigonal phase is mainly formed in the PH21-rich regions. This heterogeneous lamellar morphology with low chain connectivity between domains lowers the efficiency of stress transfer from the amorphous to the crystals, such that the onset of crystal orientation and the monoclinic-mesophase transformation are only found at higher strains. Furthermore, cavitation during deformation may occur at the interface of the phase-separated domains and may be responsible for the lower elongation at break compared to iPP/PH blends. Additional transformation of lamellar trigonals into fibrillar crystals as well as strain-induced trigonal formation in the blends of iPP/PH21 lower the level of monoclinic-mesophase transformation and act as physical joints which help the elastic recovery after removing the load.

## 4 | CONCLUSIONS

The uniaxial tensile deformation of blends of iPP and propylene 1-hexene copolymers depends on the initial semicrystalline lamellar morphology that at the same time depends on the state of the melt of the binary iPP blends. We have studied in this work the stress-strain behavior and structural transformations during deformation of melt-miscible iPP/PH11 and melt-immiscible, but partially compatible, iPP/PH21 blends in the whole range of blend composition. PH11 and PH21 are thermoplastic elastomeric random propylene 1-hexene copolymers with 11 and 21 mol% 1-hexene, respectively. These copolymers display relatively high strains at break (750-800%). Conversely, neat iPP undergoes very small tensile deformation (<5% strain).

A major conclusion of the mechanical behavior is the enhanced ductile behavior of iPP conferred by the addition of very small amounts of PH (<25%). The iPP/PH 75/25 blends reach >400% strains while maintaining the characteristic high elastic modulus of iPP. The elongation increases with increasing content of copolymer in

the blend but at the expense of a reduction of the modulus. Differences in deformation between the two types of blends at a fixed blend composition depend on the initial semicrystalline lamellar structure and unique polymorphic transformations during deformation.

iPP/PH11 blends show higher yield strength, elongation, and tensile stress at break compared to iPP/PH21 blends. Crystallization from a homogeneous melt results in mixed populations of iPP-rich and PH11-rich lamellar stacks that are highly interconnected by tie molecules of iPP and PH11 admixed in the amorphous phase. Such lamellar topology undergoes monoclinic to mesophase transformation during uniaxial tensile deformation due to effective stress transfer from the amorphous phase to the crystallites. About 25% transformation and chain orientation was observed in iPP/PH11 at elongations as low as 40%. The stress induced mesophase crystals are stable structures that remain even after removing the load. The stability of the strain-induced mesophase reduces the elastic recovery of these blends at high elongations.

Crystallization from heterogeneous melts results in separated iPP-rich and PH21-rich crystalline domains with minimum connectivity between trigonal and monoclinic stacks. Due to less effective stress transfer through the crystal stacks, a lower level of  $\alpha$ -to-mesophase transformation was observed in these blends compared to iPP/PH11 blends. Parallel to the monoclinic-mesophase transformation, strain-induced trigonal crystals form under deformation of iPP/PH21 blends due to transformation of original lamellae into a highly oriented (fibrillar) structure that serves as anchors between the mesophase and residual trigonal crystallites that may not undergo polymorphic transformation. Upon removing the load, the stress induced trigonal crystals tend to relax to random orientation, thus enhancing the elastic recovery of iPP/PH21 blends compared to iPP/PH11.

## ACKNOWLEDGMENTS

This material is based upon work supported by the National Science Foundation under Grant DMR1105129. We acknowledge the FSU High Performance Materials Institute (HPMI) for access to the X-ray diffractometer and Prof. J. Schlenoff of the Chemistry Department at FSU for access to tensile instrumentation.

## ORCID

Hamed Janani  <https://orcid.org/0000-0003-1587-2103>

Rufina G. Alamo  <https://orcid.org/0000-0002-3061-499X>

## REFERENCES

- [1] C. De Rosa, F. Auriemma, O. Ruiz de Ballesteros, L. Resconi, I. Camurati, *Chem. Mater.* **2007**, *19*, 5122.
- [2] M. H. Kim, R. G. Alamo, J. S. Lin, *Polym. Eng. Sci.* **1999**, *39*, 2117.
- [3] D. J. Lohse, *Polym. Eng. Sci.* **1986**, *26*, 1500.
- [4] H. Janani, R. G. Alamo, *J. Therm. Anal. Calorim.* **2014**, *116*, 1497.
- [5] Y. Nozue, T. Sakurai, H. Hozumi, T. Kasahara, M. Yamaguchi, M. Shibayama, Y. Matsushita, *Macromolecules* **2007**, *40*, 273.
- [6] F. Auriemma, O. Ruiz de Ballesteros, C. De Rosa, C. Invigorito, *Macromolecules* **2011**, *44*, 6026.
- [7] F. Auriemma, O. Ruiz de Ballesteros, C. De Rosa, *Macromolecules* **2010**, *43*, 9787.
- [8] L. Liu, B. S. Hsiao, B. X. Fu, S. Ran, S. Toki, B. Chu, A. H. Tsou, P. K. Agarwal, *Macromolecules* **2003**, *36*, 1920.
- [9] C. De Rosa, F. Auriemma, O. Ruiz de Ballesteros, S. D. Iacono, D. De Luca, L. Resconi, *Crystal Growth & Des.* **2009**, *9*, 165.
- [10] C. De Rosa, F. Auriemma, A. Di Capua, L. Resconi, S. Guidotti, I. Camurati, I. E. Nifantsev, I. P. Leishevstev, *J. Am. Chem. Soc.* **2004**, *126*, 17040.
- [11] Z. Cai, Y. Zhang, J. Li, F. Xue, Y. Shang, X. He, J. Feng, Z. Wu, S. Jiang, *Polymer* **2012**, *53*, 1593.
- [12] Y. Chen, S. Yang, H. Yang, G. Zhong, D. Fang, B. S. Hsiao, Z. Li, *Polymer* **2016**, *84*, 254.
- [13] H. Janani, R. G. Alamo, *Polymer* **2016**, *102*, 21.
- [14] K. Jeon, H. Palza, R. Quijada, R. G. Alamo, *Polymer* **2009**, *50*, 832.
- [15] M. Arnold, O. Henschke, J. Knorr, *Macromol. Chem. Phys.* **1996**, *197*, 563.
- [16] B. Lotz, J. Ruan, A. Thierry, G. C. Alfonso, A. Hiltner, E. Baer, E. Piorkowska, A. Galeski, *Macromolecules* **2006**, *39*, 5777.
- [17] B. Poon, M. Rogunova, A. Hiltner, E. Baer, S. Chum, A. Galeski, E. Piorkowska, *Macromolecules* **2005**, *38*, 1232.
- [18] C. De Rosa, F. Auriemma, P. Corradini, O. Tarallo, S. Dello Iacono, E. Ciaccia, L. Resconi, *J. Am. Chem. Soc.* **2006**, *128*, 80.
- [19] C. De Rosa, F. Auriemma, G. Talarico, O. Ruiz de Ballesteros, *Macromolecules* **2007**, *40*, 8531.
- [20] C. De Rosa, F. Auriemma, G. Talarico, O. Ruiz de Ballesteros, *Macromolecules* **2008**, *41*, 2172.
- [21] C. De Rosa, F. Auriemma, O. Ruiz de Ballesteros, L. Resconi, I. Camurati, *Macromolecules* **2007**, *40*, 6600.
- [22] H. Palza, J. M. Lopez-Majada, R. Quijada, R. Benavente, E. Perez, M. L. Cerrada, *Macromol. Chem. Phys.* **2006**, *206*, 1221.
- [23] C. Ruiz-Orta, J. Fernandez-Blazquez, E. J. Pereira, R. G. Alamo, *Polymer* **2011**, *52*, 2856.
- [24] H. Janani, R. G. Alamo, *Polymer* **2015**, *64*, 163.
- [25] R. G. Alamo, M.-H. Kim, M. J. Galante, J. R. Isasi, L. Mandelkern, *Macromolecules* **1999**, *32*, 4050.
- [26] I. L. Hosier, R. G. Alamo, P. Estes, J. R. Isasi, L. Mandelkern, *Macromolecules* **2003**, *36*, 5623.
- [27] I. L. Hosier, R. G. Alamo, J. S. Lin, *Polymer* **2004**, *45*, 3441.
- [28] Z. Ma, C. Shao, X. Wang, B. Zhao, X. Li, H. B. An, T. Yan, Z. Li, L. Li, *Polymer* **2009**, *50*, 2706.
- [29] C. De Rosa, F. Auriemma, G. De Lucia, L. Resconi, *Polymer* **2005**, *46*, 9461.
- [30] P. J. Flory, *Nature* **1978**, *272*, 226.
- [31] R. Popli, L. Mandelkern, *J Polym Sci B* **1978**, *25*, 441.
- [32] S. Hobeika, Y. Men, G. Strobl, *Macromolecules* **2000**, *33*, 1827.
- [33] Y. Men, G. Strobl, *J. Macromol. Sci. B* **2001**, *40*, 775.
- [34] Y. Men, J. Rieger, G. Strobl, *Phys. Rev. Lett.* **2003**, *91*, 095502.
- [35] R. Kurz, M. Schulz, F. Scheliga, Y. Men, A. Seidnitz, T. Thurn-Albrecht, K. Saalwächter, *Macromolecules* **2018**, *51*, 5831.
- [36] Y. Lu, R. Chen, J. Zhao, Z. Jiang, Y. Men, *J. Phys. Chem. B* **2017**, *121*, 6969.
- [37] Y. Lu, Y. Sun, L. Li, Y. Men, *J. Appl. Polym. Sci.* **2017**, *134*, 44747.
- [38] R. Chen, Y. Lu, J. Zhao, Z. Jiang, Y. Men, *J. Polym. Sci. Polym. Phys.* **2016**, *54*, 2007.
- [39] G. Liu, X. Zhang, Y. Liu, X. Li, H. Chen, K. Walton, G. Marchand, D. Wang, *Polymer* **2013**, *54*, 1440.
- [40] P. B. Bowden, R. J. Young, *J. Mater. Sci.* **1974**, *9*, 2034.
- [41] P. Young, R. S. Stein, T. Kyu, *J. Polym. Sci., PartB: Polym. Phys.* **1990**, *28*, 1791.
- [42] J. Kang, S. Yuan, Y. Hong, W. Chen, A. Kamimura, A. Otsubo, T. Miyoshi, *ACS Macro Lett.* **2016**, *5*, 65.
- [43] L. Santoja-Blasco, W. Rungswang, R. G. Alamo, *Ind. Eng. Chem. Res.* **2017**, *56*, 3270.
- [44] J. Zhao, Y. Sun, Y. Men, *Macromolecules* **2016**, *49*, 609.

## SUPPORTING INFORMATION

Additional supporting information may be found online in the Supporting Information section at the end of this article.

**How to cite this article:** Janani H, Alamo RG. Effect of melt miscibility, polymorphism, and crystal morphology on tensile deformation of blends of isotactic polypropylene and propylene-1-hexene random copolymers. *Polymer Crystallization*. 2020;3:e10111. <https://doi.org/10.1002/pcr2.10111>